Selectivity, Sensitivity and Detection Range in Ion-Selective Membrane-based Electrochemical Potentiometric Sensors analyzed with Poisson-Boltzmann equilibrium model

L. J. Mele, *Member, IEEE,* P. Palestri, *Senior Member, IEEE,* M. A. Alam, *Fellow, IEEE* and L. Selmi, *Fellow, IEEE*

***Abstract*— We present and validate an equilibrium model based on the Poisson-Boltzmann equations that includes the main ingredients to simulate ion-sensitive membranes in the context of electrochemical potentiometric sensors with and without ionophores. With respect to phase boundary models, our model includes spatial resolution of the electrostatic potential and concentrations. The model enables the study of Nernstian and non-Nernstian equilibrium responses, helps improving the detection range and investigating selectivity and cross-sensitivity issues related to interferent ions in the sample solution. Therefore, the model is a useful support for the design of potentiometric microelectronic sensors and helps optimizing relevant membrane features such as ionic sites and ionophore concentration for best sensitivity and selectivity.**

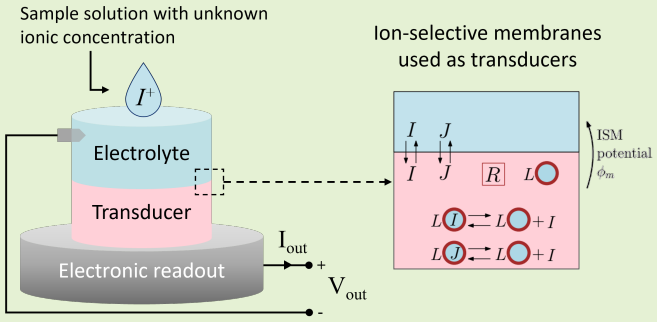

***Index Terms*— selectivity, sensitivity, cross-sensitivity, ion-sensing, potentiometric sensors, ion-selective membranes**

I. Introduction

ION-selective membranes (ISMs) are becoming the new standard in the field of potentiometric chemical sensors, given their battery-free operation, relatively fast response, low detection limit and very good selectivity [1]–[3]. ISMs may either be inserted in between two electrolyte solutions or deposited on a solid surface, i.e., ion-selective electrode (ISE) or solid-contact ISE (SC-ISE), respectively. The former configuration (ISE) is a very common setup in electrochemistry laboratories [1], [2], but requires handling two electrode/electrolyte contacts. Conversely, SC-ISEs are amenable to on-chip integration, as one side of the ISM sticks to a solid surface (e.g., a conductive polymer or the gate oxide of an ion-sensitive field-effect transistor ISFET, see Fig. 1.a) [1], [2], [4]–[6] and only one electrolyte contact is needed.

Manuscript received ——- –, 2021; revised ——- –, 2021 and —— –, 2021; accepted —— –, 2021. Date of publication ——- –, 2021; date of current version ——- –, 2021. This work was supported in part by the European Unions Horizon 2020 Research and Innovation Programme (IN-FET Project) via the IU.NET Consortium under Grant 862882 and, in part by SMART and WHIN consortium at Purdue University.

L. J. Mele and P. Palestri are with the Dipartimento Politecnico di Ingegneria e Architettura, University of Udine, Udine, UD 33100, Italy (e-mail: mele.leandrojulian@spes.uniud.it).

L. Selmi Dipartimento di Ingegneria “Enzo Ferrari”, University of Modena and Reggio Emilia, Modena, MO 41125, Italy.

M. A. Alam is with the School of Electrical and Computer Engineering, Purdue University, West Lafayette, Indiana 47907, USA.

In both implementations, the potentiometric sensor response originates at the ISM/electrolyte interface(s) and is governed by ion-transfer processes. Therefore, understanding and modeling such mechanisms is key to predicting the membrane potential. To this end, the main challenge is to include in the sensor model a robust physico-chemical description of the ISM ion exchange mechanisms as well as the chemical interactions between, e.g., ionophores in the ISM and ions from the electrolyte as sketched in Fig. 1.b. These mechanisms modify the ideal log-to-linear relation between concentration of the target analyte and ISM potential and set the lower (LDL) and upper (UDL) detection limits, hence the detection range, as illustrated in Fig. 1.c.

Several models have been proposed in the literature to interpret ISE response. The simplest is the Nikolski-Eisenman equation (NE) [7], [8] which assumes flat electrostatic potential and ion concentration profiles in the ISM and the electrolytes. These assumptions lead to what in electrochemistry are known as *phase boundary* or total-equilibrium models [1], [9]–[12], and offer a simple trade-off between complexity and usability. In equilibrium conditions, they can be successfully used to predict the logarithmic slope of the Nernstian range (e.g., $59\ \mathrm{mV/dec}$ for monovalent ionic species at room temperature). However, these models are based on semi-empirical equations and have some important drawbacks. For example, they i) fail to provide any physical insight on the

governing ion-exchange processes; ii) are difficult to integrate into full device models including, e.g., a FET; iii) may lead to inaccurate predictions for thin ISMs, where charge neutrality may not hold throughout the layer; iv) cannot capture effects such as non-Nernstian responses which can take place in equilibrium conditions and, v), do not provide time-dependent information. A complete treatment of all the aspects of the sensor operation requires that all possible interactions between ions and ISM components are appropriately accounted for.

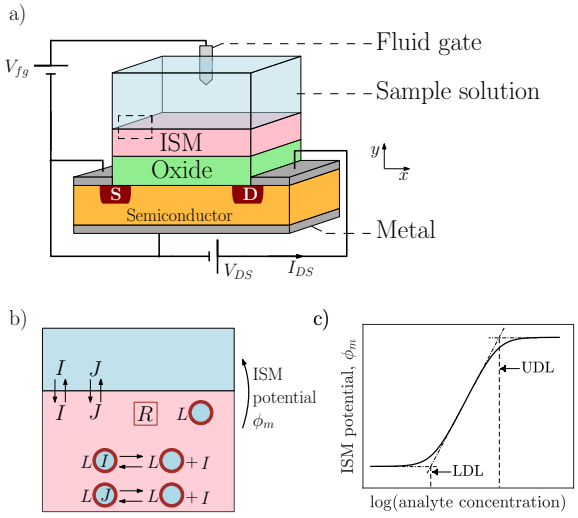

Fig. 1. (a) Example of integration of an ISM into an ISFET with indication of the electrical interconnections. (b) Zoom on the ISM/electrolyte interface (dashed rectangle in (a)), showing the main actors in the charge exchange between the two layers. Ionic sites $\boldsymbol{R}$ are sketched with squared frames whereas ionophores with circles. The latter can react with ions from the electrolyte. At equilibrium, a potential drop at the electrolyte/ISM interface, denoted as ISM potential, is formed. Its generic dependence on the bulk concentration of the (e.g., monovalent) target ionic species or analyte in log scales is shown in (c). The linear response range, or detection range, is approximately delimited by the two vertical dashed lines corresponding to the lower and upper detection limits (LDL and UDL, respectively [13]) according to the IUPAC definition [14].

Consequently, Diffusion-Layer Models [15], [16] have been used to extend phase-boundary approaches to describe the time evolution of the selectivity coefficient and LOD. However, they do not explicitly model the effect of important parameters such as ISM thickness and dielectric constants [1]. In order to address the design considerations of ISM-based potentiometry, one must self-consistently solve the drift-diffusion ion-transport, charge and current continuity together with the electrostatics described with the Poisson equation. This leads to what are called Nernst-Planck Poisson (NPP) models in the analytical chemistry community [17]–[21]. Nevertheless, one should consider that time-dependent simulations are computationally demanding and not versatile for extensive sensor optimization across many unknown parameters.

In this work, we provide a general modeling framework using the well-known Poisson-Boltzmann formalism that is capable of handling an arbitrary number of ions with any valence charge as well as including ionophores that interact with up to two ionic species. The adopted formulation can be used to address features like selectivity and sensitivity (as in phase boundary models), but adding one spatial dimension with relatively low computational cost. Adding more physical dimensions is possible, but it does not provide additional insights because given the typical dimensions of the membranes and typical concentration ranges, 1D models are accurate enough. Differently from the models typically employed in analytical electrochemistry, the proposed approach spatially resolves the electrostatic potential, making it suitable for integration with FET device solvers and complete sensor simulations.

The manuscript is divided in two parts, respectively devoted to ISM analysis without and with inclusion of ionophores. The former case is presented in Section II, where a one-dimensional Poisson-Boltzmann model of the ISM/electrolyte system at equilibrium is introduced. Intrinsic membrane selectivity to ions (as a result of different membrane affinity) and comparison with experimental data are shown as well. In the second part, Section III, distributed chemical reactions between ionophores and ions in the electrolyte are added to the former model. The simulation deck is validated against experimental data including cross-sensitivity issues in presence of interferent ions and features such as selectivity (expressed via the selectivity coefficient K_{IJ}^{POT}), optimum ionophores-to-ionic sites concentration ratio, UDL, LDL and detection range are addressed with numerical examples. Pros and cons of our approach are finally discussed in Section IV.

II. ISM/ELECTROLYTE SYSTEMS WITHOUT IONOPHORES

A. Poisson-Boltzmann modeling framework

Let us first consider the ion-transfer processes across the membrane/electrolyte interface, that define the response in ISM-based biosensors [1]. For simplicity, we exclude the semiconductor part of the device to highlight processes and voltage drops at the membrane/electrolyte interface. Clearly, the full system has additional electrostatic potential drops, but they are independent of the chemical composition of the sample. We have shown in [22] that the response of the sensing element and the FET behavior can be decoupled, i.e., the threshold voltage shift can be safely obtained modeling the sensing element alone. We use concentrations in place of activities assuming full dissociation of salts and neglecting the discrete nature of ions [11]

When the system is *at equilibrium*, Boltzmann statistics applies in the low concentration limit. The space-dependent concentration $[i]$ in the electrolyte of the species 'i' with signed valence z_i, hereafter denoted $[i^{z_i}]$ is:

$$[i^{z_i}]\,(y \in \mathrm{el}) = [\mathrm{i_B^{z_i}}] \exp\left(-\frac{\mathrm{z_i q}}{\mathrm{k_B T}}\left(\psi\,(\mathrm{y}) - \mathrm{V_{fg}}\right)\right), \quad (1)$$

where $[i_B^{z_i}]$ is the concentration in molar units M in the bulk of the electrolyte (i.e., in the neutral region far from the ISM), q denotes the absolute electron charge, k_B is the Boltzmann constant, T the temperature and V_{fg} is the potential in the bulk of the electrolyte taken as reference (e.g., set by the fluid gate in Fig. 1.a). The electrolyte domain is taken much larger than the Debye length so that concentrations and potential in the bulk are essentially constant.

When membrane and electrolyte are brought into contact, one needs to take into account the affinity step between two media (denoted as *single ion distribution* in the

electrochemical terminology [10], [23]) defined as $k_i = \exp(\Delta\mu^0/N_A k_B T)$, with $\Delta\mu^0$ being the difference of standard chemical potential between the ISM and electrolyte phases for ion 'i' and N_A is Avogadro's constant. The Boltzmann distribution in the membrane phase reads:

$$[i^{z_i}]\,(y \in \mathrm{ISM}) = \mathrm{k_i}\,[\mathrm{i_B^{z_i}}] \exp\left(-\frac{\mathrm{z_i q}}{\mathrm{k_B T}}\left(\psi\,(\mathrm{y}) - \mathrm{V_{fg}}\right)\right). \quad (2)$$

The value of k_i depends on the polarity of the ISM solvent. For example, membranes with low polarity (low dielectric constant) have low affinity values, since ion-transfer processes from the electrolyte (i.e., a hydrophilic phase with high dielectric constant) is not favorable. Other ionic properties such as valence charge and size also play an important role. In fact, small multi-valent ions (e.g., Ca^{2+}) are more polar and therefore experience higher energy barrier when transferred into a lipophilic ISM [13]. Such a simple concept explains the *intrinsic* selectivity of ISMs to different ions and is well-described by the Hofmeister series [24], i.e., a series of cations (or anions) sorted from high to low affinity to lipophilic phases.

The electrostatic potential entering Eqs. 1, 2 depends on the total charge density distribution over space according to the Poisson equation,

$$\frac{d}{dx}\left(\varepsilon(y)\frac{d\psi(y)}{dx}\right) = -\Big(\rho_m\,(y) + \rho_f\,(y)\Big), \quad (3)$$

where $\varepsilon(y)$ is the electrical permittivity of the medium (which depends on complex local polarization phenomena [25]), ρ_f the fixed charge density (see Section II-B), and the charge density of the mobile ions, ρ_m, is calculated as

$$\rho_m(y) = qN_A \sum_i z_i[i^{z_i}](y). \quad (4)$$

Combining the Poisson equation with Eqs. 1, 2 we obtain the non-linear Poisson-Boltzmann (PB) equation, that describes the system at equilibrium [26].

It is worth noting that the PB model is an equilibrium model. Its solution is rigorously equal to a steady-state condition only in the case of a blocking interface. For ISMs located in between two electrolytes (e.g., in conventional ISEs) non-null single ion fluxes can exist across the membrane even if the total current is null, leading to a steady state configuration that does not correspond to equilibrium, with the presence of possible diffusion potentials. These latter do not appear with blocking interfaces where equilibrium and steady state mean that every single ion has zero net current.

Figure 2 gives numerical proof that the time-dependent NPP model solution converges to our PB model for $t \to \infty$. The NPP simulations were carried out using the online-available NPP solver JEDS [27] assuming the structure depicted in Fig. 3.a, where one side of the ISM is blocked. The computational burden of our PB models is orders of magnitude less than the NPP model, so if a steady-state solution is required, the PB approach is much more efficient than running the NPP model since the transient converges.

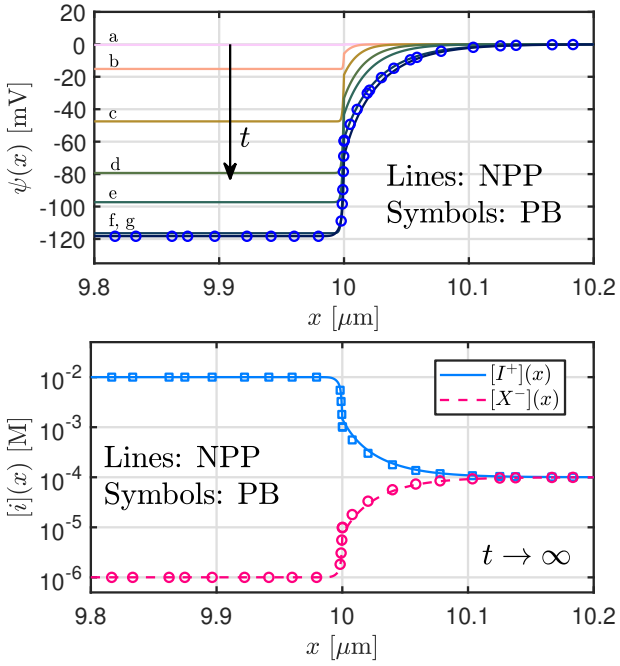

Fig. 2. Top: electrostatic potential across the ISM/electrolyte interface, obtained from the NPP solver JEDS [27] (lines) and from our PB model (symbols). NPP solutions are reported for different time frames showing the progressive convergence to the PB model: (a) **0** s, (b) **50** ns, (c) **200** ns, (d) **500** ns, (e) **1** μs, (f) **300** s, (g) **1800** s. The simulated structure is sketched in Fig. 3.a with ISM and electrolyte layer thickness of **10** μm. Other parameters are: $[\boldsymbol{IX_B}]$=**0.1** mM, $[\boldsymbol{R^-}]$=**10** mM, $\boldsymbol{k_I}$=$\boldsymbol{k_X}$=**1**. For the NPP solver, we used the diffusion coefficients values $\boldsymbol{D_I}$=$\boldsymbol{D_X}$=$\boldsymbol{10^{-9}}$ $\mathbf{m/s^2}$ in the electrolyte and, $\boldsymbol{D_I}$=$\boldsymbol{D_X}$=$\boldsymbol{10^{-11}}$ $\mathbf{m/s^2}$ and $\boldsymbol{D_R}$=**0** $\mathbf{m/s^2}$ in the ISM. Bottom: concentration profiles from PB are compared to NPP for $\boldsymbol{t \to \infty}$.

B. Study of ionic sites and ion affinity

In order to operate as potentiometric sensors, ISMs are doped with so-called *ionic sites* or *ion-exchangers*, i.e., charged lipophilic ions with very low mobility or covalently fixed to a polymeric matrix [12]. Ionic sites are essentially confined in the ISM phase, while ions can be exchanged via drift and diffusion across the ISM/electrolyte interface (see Fig. 3.a). In particular, if the concentration of positive and negative ions in the electrolyte is lower than the one of ionic sites in the ISM, then, at equilibrium, the ions with the same charge sign as ionic sites (e.g., negatively charged X^- ions in Fig. 3.a, hereafter called *co-ions*) diffuse into the membrane in a relatively small amount due to the repulsive electric field exerted by the ionic sites. Conversely, ions with opposite charge (i.e., *counter-ions* I^+ in Fig. 3.a) are attracted by the ionic sites, so that their concentration in the ISM counter balance the combined effect of the ionic sites and its co-ions. Hence, as long that these conditions are met, the concentration of the counter-ion I^+ is fixed by the ionic sites' concentration $[R_R^z]$ regardless of their concentration in the sample solution, $[I_B^{z_I}]$. The potential step at the electrolyte/ISM interface, or *membrane potential*, then follows Nernst equation

$$\phi_m = \frac{k_B T}{q z_I} \ln \frac{k_I [I_B^{z_I}]}{[I_{ISM}^{z_I}]} \approx \frac{k_B T}{q z_I} \ln \frac{k_I [I_B^{z_I}]}{[R^{z_R}]}, \quad (5)$$

where $[I_{ISM}^{z_I}]$ denotes the concentration of species I in the bulk of the ISM. In Eq. 5, the maximum sensitivity for monovalent

ions at 300 K is ≈ 59 mV/dec.

To investigate the validity limits of Eq. 5 with our model (Eqs. 1-3), we firstly simulate the ISM/electrolyte junction sketched in Fig. 3.a by setting $V_{fg} = 0$ V at the liquid gate and Neumann boundary conditions (i.e. zero electric field, similar to [10]) at the electrode/ISM interface. The relative electrical permittivity of the electrolyte and the ISM related to low-frequencies are fixed to 79 and 4.8, respectively [13], [28] and the temperature to 298.16 K. For simplicity, ionic sites R^{z_R} are considered as uniformly distributed fixed charges (even though non-uniform distributions are also possible) giving a volumetric charge density $\rho_f = qN_A z_R[R^{z_R}]$ in Eq. 3. These settings are common to all calculations in this manuscript unless otherwise specified.

Figure 3.b reports the membrane potential of a cation-selective membrane (i.e., one with negatively charged ionic sites) for different concentrations of the dissociated salt I^+X^- in the sample and unitary affinity constants. We observe that for low concentrations of $[IX_B]$, the membrane potential is proportional to the log of $[I_B^+]$, where the proportionality factor is lower than in Eq. 5 for concentrations of $[IX_B]$ that approach the one of ionic sites $[R^-]$ and eventually becomes zero, thus approximately setting the UDL to the ionic site concentration $[R^-]$. This effect is also seen in Figs. 3.c and (d), that show the spatial profiles of the concentrations and potential at three simulations points marked with black stars in plot (b). As shown by dotted lines, the membrane potential (i.e., the built-in electrostatic barrier) becomes zero when the co-ions concentration $[X^-]$ (and so the target ions one $[I^+]$) are much larger than $[R^-]$ in the electrolyte and the ISM, meaning that they can freely diffuse in the membrane leading to *Donnan exclusion failure* [14]. Differently, in the range of log-to-linear response in plot (b) the concentration of co-ions X^- (dashed and solid lines with circles in plot c) is much lower than $[R^-]$ in the ISM, which allows one to make the approximation $[I^+_{ISM}] \approx [R^-]$ as in Eq. 5 and therefore obtain Nernstian response.

The impact of the concentration of ionic sites $[R^-]$ in the ISM can be observed comparing the line with red circles and the one with blue squares in Fig. 3.b, where $[R^-]$ is varied over one decade. The log-to-linear relationship is clearly observable over ranges that increase with $[R^-]$. Indeed, the larger the concentration of ionic sites, the higher the concentration of I^+X^- at which the co-ions X^- diffusing into the membrane kill the sensitivity to I^+.

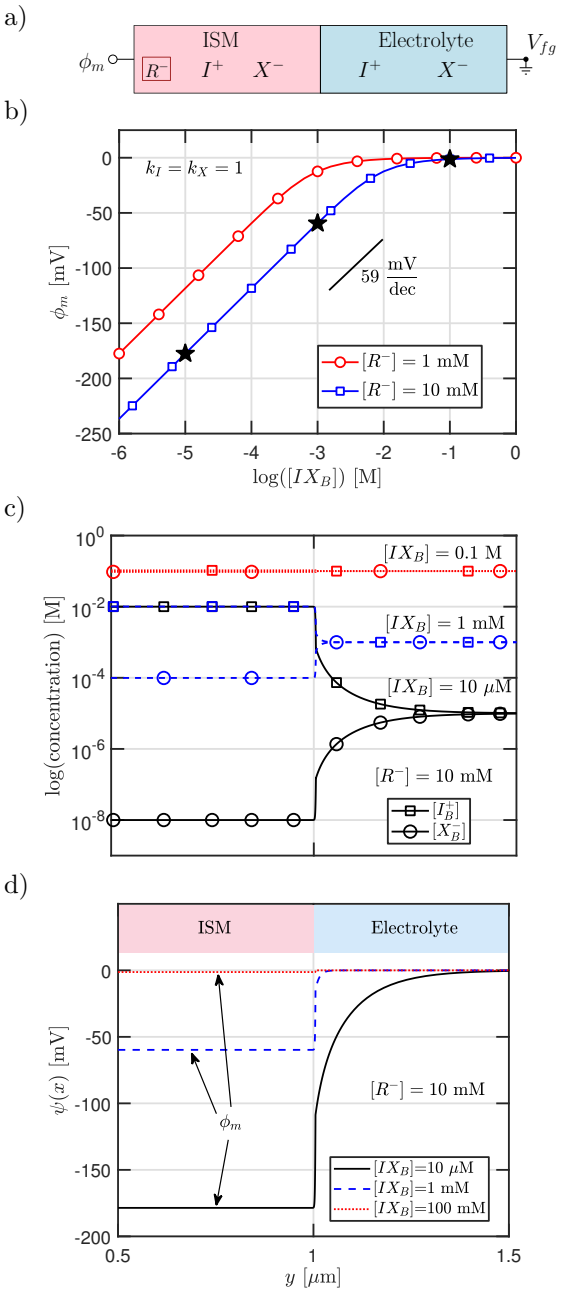

Fig. 3. (a) Sketch of the considered structure with indication of the involved ions and electrodes. (b) Simulated membrane potential vs the concentration of I^+X^- salt in the electrolyte for two different concentrations of ionic sites. The simulations refer to unitary affinity constants, i.e., $\boldsymbol{k_I = k_X = 1}$. The concentration of the ionic species and potential profiles at the ISM/electrolyte interface, relative the points marked with black stars in (b), are reported in (c) and (d), respectively.

C. Study of the detection range and selectivity

To go further into the previous analysis we focus on the limits of the Nernstian response, i.e., the UDL and LDL that define the detection range. According to IUPAC definition [14], the UDL is equal to the concentration of ionic sites in the ISM. However, this is valid only for unitary affinity coefficients. Figure 4.a reports simulations as in Fig. 3.b but with different choices of k_I and k_X while fixing $[R^-] = 10$ mM (i.e., to typical values used in experiments [5], [9], [10], [13], [29]). With respect to $k_I = k_X = 1$ (red curve with circles), we observe a tenfold increase of the UDL for either, i), a hundredfold decrease of only k_I (green line with squares) or, ii), a hundredfold decrease of only k_X (blue line with diamonds) or, iii), a tenfold decrease of both k_I and k_X (black line with triangles), suggesting that the UDL is fairly approximated by $UDL \approx [R^-]/\sqrt{k_I k_X}$, where the square root arises from the fact that $[X_B^-]$=$[I_B^+]$=$[XI_B]$. In a more general case, it can be easily derived that:

$$\log UDL = \log [R^-] - \log (z_I k_I k_X) - \log [X_B^-]. \quad (6)$$

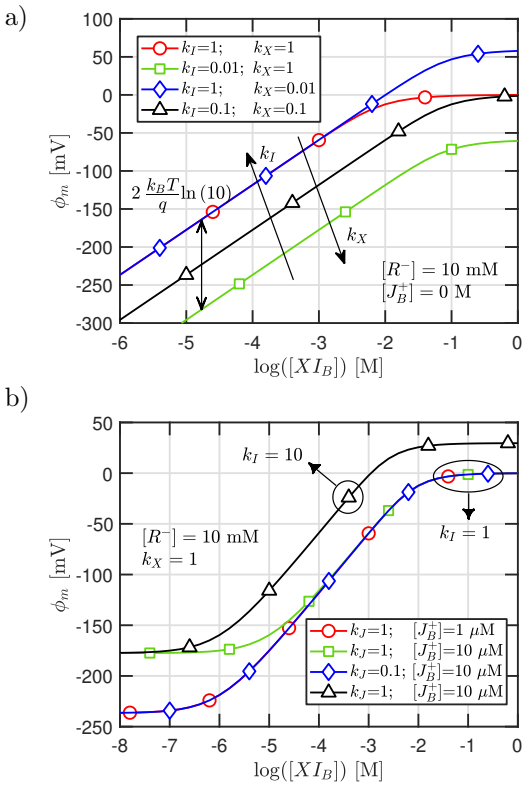

Fig. 4. Simulated membrane potential vs the I^+X^- salt concentration in the sample for different choices of the affinity constants, without (a) and with (b) the generic interferent cation J^+ in the sample electrolyte.

Interestingly, the membrane potential values at the plateaus in Fig. 4.a range from negative to zero to positive values if we scale only k_I, both k_I and k_X or just k_X, respectively. The reason is given by the imparted ISM (intrinsic) selectivity, that results into a spontaneous accumulation of the ionic species with higher affinity value into the ISM and, therefore, the formation of a potential barrier that has the same sign of the excess ion's valence charge.

In order to study the LDL, we introduce in the simulations an additional counter-ion J^+ (hereafter called *interferent* ion) different from the target I^+. As shown in Fig. 4.b, when k_I=k_J=k_X=1 (red line with circles and green line with squares), i.e., when target ion and interferent ion have the same affinity, a plateau takes place for $[I_B^+] \ll [J_B^+]$ and a membrane response to ion I^+ is therefore obtained in the range $[J_B^+] \ll [I_B^+] \ll [R^-]$. The effect of changing the affinity constants are instead reported by the blue line with diamonds and black line with triangles in Fig. 4.b. In the first case, the tendency of LDL increase due to a higher concentration of the interferent ion J^+ is compensated by a lower affinity value of the same ion, thus suggesting that the LDL is proportional to $k_J[J_B^+]$. In the second case, a tenfold increase of k_I lowers the LDL leading to a $\propto 1/k_I$ relationship. This behavior can be expressed using thermodynamic considerations. When Nernst conditions holds (see Eq. 5), one can demonstrate that

$$\log LDL = \frac{z_I}{z_J}\log\left(z_J k_J [J_B^{z_J}]\right) - \log\left(z_I k_I\right) + \\ + \left(1 - \frac{z_I}{z_J}\right)\log[R]. \quad (7)$$

Equation 7 has been verified numerically with our model for a large number of cases (not shown). Moreover, since the condition of Nernstian response is necessary when determining the ISM selectivity as in, e.g., separated solution method (SSM) or fixed interference method (FIM) [30], [31], one can use Eq. 7 to derive a model for the potentiometric selectivity coefficient [31]:

$$\log K_{IJ}^{POT} = \frac{z_I}{z_J}\log\left(z_J k_J\right) - \log\left(z_I k_I\right) + \left(1 - \frac{z_I}{z_J}\right)\log[R]. \quad (8)$$

where we note that not just ionic properties such as ion valence charges and affinity constants affect the potentiometric selectivity coefficient, but also the concentration of ionic sites when $z_I \neq z_J$. This is in accordance with what was previously suggested in [32], [33] and experimentally observed in [34]. The selectivity values relative to the cases in Fig. 4.b, calculated using Eq. 8 are reported in Table I together with other numerical examples. We see that Eq. 8 is in good agreement with the K_{IJ}^{POT} extracted directly from the simulated ϕ_m vs $[XI_B]$ using the method described in [31].

TABLE I
POTENTIOMETRIC SELECTIVITY COEFFICIENTS FOR DIFFERENT ISM PARAMETERS.

$[R]$ (mM)	10	10	10	10	1	10	1
k_I	10	1	1	1	1	1	1
k_J	1	1	0.1	1	1	1	1
z_I	1	1	1	1	1	2	2
z_J	1	1	1	2	2	2	2
$\log K_{IJ}^{POT}$ [a]	-1	0	-1	-0.9	-1.4	0	0
$\log K_{IJ}^{POT}$ [b]	-1	0	-1	-0.9	-1.5	0	-0.1

[a] Calculated using Eq. 8. [b] Calculated using [31, Eq. 5] with the LDL values extracted from our simulations.
The first three columns refer to the same cases analyzed in Fig. 4.b.

D. Comparison with experimental data

Curves as those in Fig. 4.b are very often observed in experiments when performing calibration, i.e., consecutive membrane potential measurements upon consecutive dilutions of the target ion concentration in the sample. Following the experimental work in [29], we consider a cation-sensitive ISM with thickness of 200 μm and $[R^-] = 5$ mM. The sample solution consists is a mix between a salt containing the cation tetramethylammonium, TMA^+, and salts with the generic interferent cation with concentration $[J_B^+] = 2$ mM (with J^+ being one among K^+, Na^+ and Ca^{2+}). By plugging these parameters in the PB model described in Section II-A, excellent agreement is found between simulations and the experimental data in [29], as reported in Fig. 5 (lines vs symbols, respectively). It should be noted that to compensate for the missing inner reference solutions in the experiments in [29], we solve the junction between membrane and reference solution and subtract it from the simulation of the membrane/sample solution junction. A direct consequence of this simulation procedure is that the derived affinity constants of the interferent ions in Fig. 5 are relative to k_{TMA} (ultimately set to 0.0043 from the standard Gibbs free energies reported

in [35]), since the computed potential in the absence of interfering ions only depends on the ratio between [TMA$^+$] in the sample and reference solutions and not on k_{TMA}. The values of k_J that we have set in the simulations in order to reproduce the experiments in the presence of interferent ions are consistent with the Hofmeister series [24]: for example, K$^+$ is the most lipophilic ion among the selected interferents (i.e., has the highest affinity constant) and therefore sets the LDL to a relatively high concentration of the target ion, TMA$^+$. Interestingly, a LDL is also observed when no interferent ions are intentionally added (black symbols in Fig. 5). This could be explained with the possible contamination of K$^+$ ions from the KCl bridge electrolyte contacting the reference half-cell [29]. In fact, more than satisfactory agreement with simulations was obtained by adding potassium ions as the interfering cation with concentration $[K^+] = 11\ \mu$M.

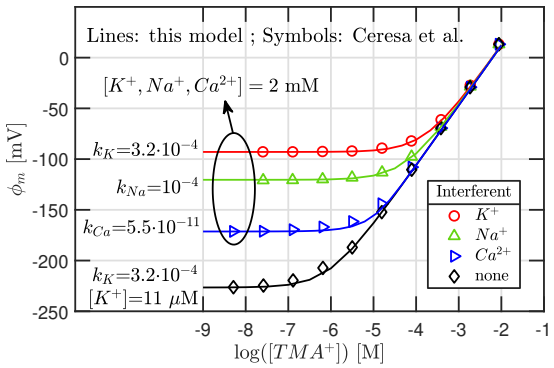

Fig. 5. Experimental (symbols, [29]) vs simulated (lines) calibration curves of TMA$^+$ for a cation-selective membrane in the presence of different interferent ions. The ISM was composed by sodium tetrakis-[3,5-bis(trifuoromethyl-phenyl]borate (NaTFPB, in **0.45** wt%, **5.00** mmol/kg), bis(2-ethylhexyl) sebacate (DOS, in **66.15** wt%), and Poly(vinyl chloride) (PVC, in **33.40** wt%). In the simulations, chloride ions Cl$^-$ were used to provide electroneutrality in the sample electrolyte.The affinity constants that yield the best fit are reported in the figure whereas $\boldsymbol{k_{TMA} = 0.0043}$ and $\boldsymbol{k_{Cl} = 2{\cdot}10^{-9}}$ were set from [35]. For the case without intentionally added interferent ions (black symbols and line) we assumed interference from K$^+$ ions with $\boldsymbol{[K^+] = 11\ \mu}$**M** due the KCl bridge salt in [29].

III. ISM/ELECTROLYTE SYSTEMS WITH IONOPHORES

A. Inclusion of chemical reactions into the PB model

Figure 5 in Section II demonstrated that interferent ions with high affinity constant (if present with relevant concentrations) reduce the detection range of the sensors. To prevent this, one can add in ISMs the so-called *ionophores*. These are mobile, charged or neutral lipophilic compounds that form complexes with ions at the ISM/electrolyte interface, imparting artificial selectivity to the ISM according to the specific ion-ionophore binding affinities. The charge of the complex contributes to the potential barrier ϕ_m as well.

In ISMs, the concentration of ionophores is typically comprised in the range of 0.5-2% of the membrane mass [13], meaning that ISMs' mechanical properties are not significantly modified upon their mixing with ionophores. Furthermore, the majority of ionophores employed in ISMs are neutral and their effect on the electrical permittivity is minimum.

Based on the experimental observations, ionophores have been considered in phase boundary models for ISEs [9], [10], [12], [36], [37], where one or more ionophores can react with a single ion (target of interferent) according to the binding stoichiometric coefficients.

In this section, we extend to one dimension the theory in [10], that includes reactions between one type of ionophore and two ionic species, namely, the target ion I and the interferent ion J, respectively. Models considering more than one interferent species [9], [12], [37] can be implemented in a similar way, but are not discussed in this work.

Under these assumptions, inclusion of ionophores in the PB model results in an extra set of equations to define the space charge density in the domain. The binding/unbinding reactions between free ions, I and J, and ionophores, L, inside the membrane are then

$$\begin{aligned} I^{z_I} + n_I L^{z_L} &\leftrightharpoons IL_{n_I}^{z_{IL}} \\ J^{z_J} + n_J L^{z_L} &\leftrightharpoons JL_{n_J}^{z_{JL}}, \end{aligned} \tag{9}$$

where n_I and n_J are the stoichiometric coefficients for a single primary or interfering ion, respectively, while $z_{IL} = z_I + n_I z_L$ and $z_{JL} = z_J + n_J z_L$. The products are the $\mathrm{IL_{n_I}}$ and $\mathrm{JL_{n_J}}$ complexes, respectively. At equilibrium, the complexes formed between ionophores and electrolyte ions depend on the association constants β_{IL} and β_{JL}, respectively [10]:

$$\beta_{IL} = \frac{[IL^{z_{IL}}](y)}{[I^{z_I}](y)\,[L^{z_L}]^{n_I}(y)}, \quad \beta_{JL} = \frac{[JL^{z_{JL}}](y)}{[J^{z_J}](y)\,[L^{z_L}]^{n_J}(y)}. \tag{10}$$

Normally, ionophores are mobile and strongly lipophilic molecules; ideally, they do not escape from the membrane phase. Therefore, their total quantity remains fixed and mass conservation should be included in the model, i.e., the space integral of the concentration of ionophores should remain constant. However, it can be shown that for nowadays typical ISM thicknesses (much larger than the Debye screening length) and at the equilibrium a constant concentration of ionophores can be assumed throughout the space, without appreciable loss of accuracy. This simplification is expressed as:

$$[L_{tot}] = [L^{z_L}](y) + n_I\,[IL^{z_{IL}}](y) + n_J\,[JL^{z_{JL}}](y), \tag{11}$$

where $[L_{tot}]$ is the total concentration of ionophores (free and bound). Since the space dependency of free and bound ionophores is solely dictated by the distributed chemical reactions, ρ_f in Eq. 3 now reads:

$$\begin{aligned} \rho_f(y) = qN_A \big(&z_R[R^{z_R}] + z_{IL}[IL_{n_I}^{z_{IL}}](y) \\ &+ z_{JL}[JL_{n_J}^{z_{IL}}](y) + z_L[L^{z_L}](y)\big). \end{aligned} \tag{12}$$

Conversely, unbound ionic species I and J in Eq. 10 still follow Boltzmann statistics, Eq. 2.

By inserting Eq. 11 into Eq. 10 one obtains a system of two equations for the two unknown concentrations of complexed species IL and JL, respectively:

$$\begin{cases} [IL] &= \beta_{IL}\,(L_{tot} - n_I\,[IL] - n_J\,[JL])^{n_I}\,[I] \\ [JL] &= \beta_{JL}\,(L_{tot} - n_I\,[IL] - n_J\,[JL])^{n_J}\,[J], \end{cases} \tag{13}$$

where, for the sake of a simpler notation, we dropped the ionic valences of free and complexed ions as well as the spatial

dependence y. Hence, by inserting Eq. 2 into Eq. 13 and solving one obtains the expressions for $[IL]$ and $[JL]$ as a function of the electrostatic potential. In fact, the electrostatic potential appears in the expression of all unbound species' concentrations according to the Boltzmann factor.

Since Eqs. 13 contribute to the fixed charge density of the ISM (Eq. 12) they must be computed at each iteration of a self-consistent (e.g., Newton-Raphson) loop given by Eqs. 1-4, 12. The complexity of such a task rapidly increases with stoichiometric coefficients other than '1', especially when calculating the Jacobian terms. In this work, we used a symbolic solver to find the analytical expressions of $[IL]$ and $[JL]$ complexes in Eq. 13 and their Jacobian terms when $n_{I,J} = 2$ and 3. An implementation flowchart of the PB model including ionophores is reported in Fig. 6. We have shown in [38] that the membrane potential provided by our model with ionophores is in perfect agreement with the model in [10] over a wide variety of ISM parameters. With respect to [10], our model does not only provide the membrane potential but the entire potential and concentration profiles $\psi(x)$ and $[i](x)$.

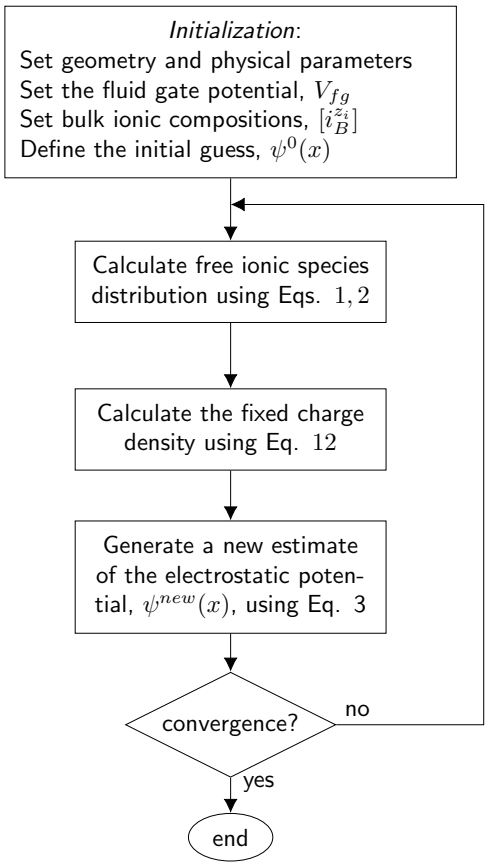

Fig. 6. Flowchart of the algorithm used to implement the PB model with distributed chemical reactions between ionophores and ions.

B. Validation with experimental data

In this Section, we compare the model in Section III-A with the experiments reported in [5], for a calcium-sensitive ISFET (Fig. 1.a). In [5], the measurements with both the target and interferent ionic species were performed using the ionophore ETH 1001 –3%, and ISM composition consisting of polymeric tripropyleneglycol diacrylate pol(TPGDA) –54.8%, bis(2-ethylhexyl)sebacate (DOS) plasticizer –40.6%, and tetrakis(p-chlorophenyl)borate KTpClPB ionic sites –1.6%.

TABLE II
PARAMETER VALUES USED IN THE SIMULATIONS IN FIG. 7.

Symbol	Value	Units	Symbol	Value	Units
ε_{el}	80	-	β_{CaL_2} [a]	10^{19}	M^{-2}
ε_m	4.8	-	β_{MgL} [b]	$8{\cdot}10^{13}$	M^{-1}
k_{Ca}	$5.5{\cdot}10^{-11}$	-	$[Mg^{2+}]$ [b]	100	mM
k_{Cl}	$2{\cdot}10^{-9}$	-	$[R^-]$	10	mM
k_{Mg} [b]	$1.6{\cdot}10^{-11}$	-	$[L_{tot}]$	22	mM

[a]Value taken from [39]. [b]For $MgCl_2$ only.

The ISM potential computed with our model using the parameter values in Table II (where k_{Ca}, k_{Cl} and dielectric constants are the same as in Fig. 5) is compared in Fig. 7 with the experimental data from [5] (lines vs symbols, respectively) for two different background electrolytes: pure $CaCl_2$ solutions (red squares) and a mixed solution with $CaCl_2$ and $MgCl_2$ (blue circles). In the simulations, we used a 1:2 stoichiometric coefficient for Ca^{2+}-ionophore complex according to [5], [40] (i.e., n_I=2 in Eq. 13) while 1:1 stoichiometry has been assumed for the interfering Mg^{2+}-ionophore (i.e., n_J=1). The background concentration of chloride ions was adjusted to achieve electroneutrality in the electrolyte sample.

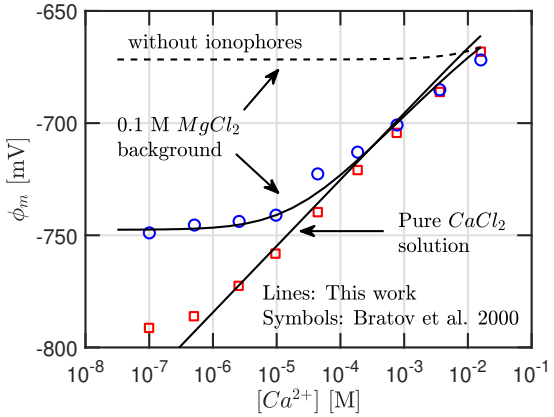

Fig. 7. ISM membrane potential ϕ_m vs the calcium concentration in the electrolyte in an ISFET structure. Symbols show the experimental data reported in [5] whereas solid and dashed lines are the simulations of this work. For the sake of an easier comparison, the chosen x-axis orientation is consistent with other plots in this manuscript rather than with [5]; furthermore, simulation results are all rigidly shifted by the same amount along the y-axis to be comparable to the fluid gate potential measurements. The simulation parameters are reported in Table II.

As shown in Fig. 7, Nernstian response (i.e., $\approx$ 29.5 mV for a divalent ion) is obtained for pure $CaCl_2$ over almost the whole range of explored concentrations, with a slight tendency to saturation for $[Ca^{2+}] \lesssim 10^{-6}$ M, due to possible interferent with ionic impurities. For the second background electrolyte ($CaCl_2$ and 0.1 M of $MgCl_2$), the ISFET response from the experimental data (blue circles) is, once again, nicely reproduced by our simulations (solid line).

The importance of the ionophores in determining the selectivity is exemplified by the dashed line in Fig. 7. We observe that, without ionophores, Mg^{2+} ions inflect the response curve below 10 mM and completely flatten the ISM response below $[Ca^{2+}] = 10^{-3}$ M.

C. Effect of ionophores on selectivity

Once validated, the simulation model can be used to predict the response of the sensor to different ionic combinations to study the impact of any parameter on the system. For instance, as reported in [10], [38], sub, inverted and super-Nernstian ISM equilibrium potentials can be obtained as a result of specific stoichiometric coefficients of ion-ionophore complexes and the ionic valences.

In this Section, we derive interesting insights concerning the effect of the ion-ionophore stability on the typical sensor response (e.g., Fig. 1.c). To this aim, we consider a cation-selective ISM containing negatively charged ionic sites $[R^-]$ (and therefore repelling anions) and temporarily assume ionophores with a total concentration, $[L_{tot}]$ in a 2:1 proportion with respect to ionic sites. In the following examples, we focus on neutral ionophores (the most common case) and set the ionic affinity coefficient for all ions to one. The reason of the latter choice is to avoid imparting an intrinsic selectivity to the ISM (see the dependencies of UDL and LDL on k_I, k_J and k_X shown in Sections II-B and II-D) so to focus only on the effects given by the ionophores.

In the first analysis, we assume $\beta_{JL} = 0$ M^{-1} and, therefore, $[JL^+] = 0$ M. The corresponding membrane potential is reported with black lines in Fig. 8 for different values of the association constant β_{IL}. Results show that, increasing the binding strength of the IL complex, hence unbalancing the reaction towards the bound IL configuration both the LDL and UDL shift towards lower primary ion concentrations (see Section III-E). On one hand, a lower LDL means increased sensitivity and thus the capability of sensing the concentration of target ions at lower concentrations with respect to ionophore-free ISMs (line with circles in Fig. 8.a). On the other hand, lower UDL means that saturation of free ionophores occurs at lower concentrations of the target ionic species. Since ionophores are generally in excess with respect to ionic sites, the saturation is preceded by a sign change of the membrane potential (e.g. from negative to positive in the considered example). Such change is anticipated to lower $[IX_B]$ concentration for higher values of β_{IL}, and electrostatically forces the extraction of co-ions (X^-) from the electrolyte to the ISM, well before that the diffusion-related Donnan exclusion failure takes place. A direct consequence of this is the formation of an inverted-Nernstian response after the onset of UDL [12], [41], [42].

In order to better understand the above phenomena, Figs. 8.c and d report the ionic concentration profiles across the ISM/electrolyte structure sketched in Fig. 8.b when $\phi_m = 50$ mV and $[I_B^+]$ lies below and above the UDL, respectively. In the first case (Fig. 8.c), ionic sites are the dominant anions in the ISM and are compensated by IL^+ complexes that, in turn, fix the concentration of I^+ in the membrane through the reaction equilibrium, therefore providing Nernstian relationship

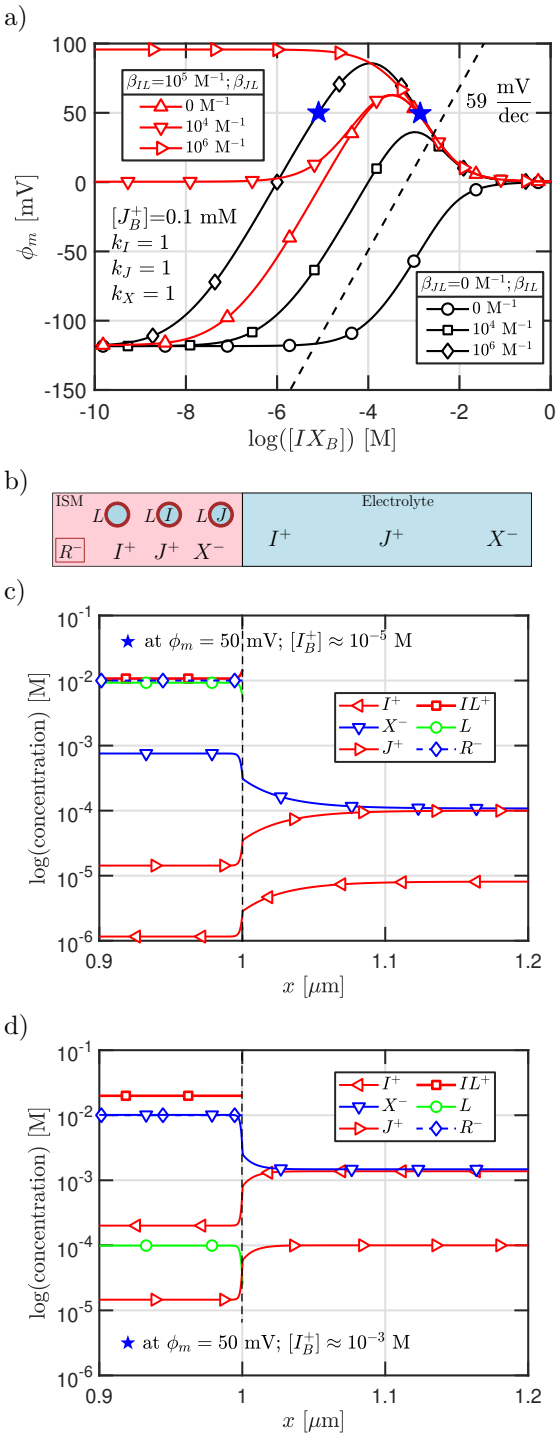

Fig. 8. (a) Black curves: calibration curves of ISMs at equilibrium containing ionophores perfectly selective to the target ion I^+, for different values of the association constant β_{IL}. Red curves: same as black curves but varying β_{JL} for $\beta_{IL} = 10^5$ M^{-1}. $[R^-] = 10$ mM and $[J_B^+] = 0.1$ mM. In (b) and (c) the spatial ionic concentration profiles relative to the calibration point marked with blue star symbols in (a) (i.e., when $\phi_m = 50$ mV) are shown, respectively.

to changes of $[I_B^+]$. Also, the concentration of free ionophores L (green lines with circles) in the ISM is comparable to that of complexed ones.

In the second case (Fig. 8.d) instead, almost all ionophores are in the complexed state IL^+. The consequences are two-

fold: firstly, since ionophores are saturated, ions I^+ enter the ISM in the free form and their concentration is no longer fixed in the membrane. Secondly, the new IL^+ complex behaves as the original R^- ionic sites, except being sensitive to anions, rather than cations. This leads to the observed inverted Nernstian response, that eventually vanishes when the concentration of anions X^- is greater than that of IL^+ complexes in the membrane ($\approx [L_{tot}]$ in saturation conditions, as shown by red lines with squares in Fig. 8.d).

Despite the condition of perfect ionophore selectivity used in this virtual experiment, the effect of free interferent ions J^+ reveals itself at very low concentrations of the primary ions, setting the LDL. This holds true regardless the binding strength β_{IL} which can reduce but not eliminate the LDL.

We now analyze the reaction between interferent ions and ionophores, making cross-sensitivity issues to become more relevant. The main consequence is that the ability of the ISM to set the concentration of target ions is reduced and the range of maximum sensitivity shrinks. Of course these effects depend on the stability (or association constant) of the target and interferent ion-ionophore complex as well as the concentration of the species in the sample electrolyte. To show this, let us reconsider the previous analysis and allow the formation of JL^+ complexes. The resulting membrane potential is shown by red lines with triangles in Fig. 8.a, for different binding constants of the interferent ion-ionophore complex, β_{JL}, while keeping $[J_B^+] = 0.1$ mM and setting β_{IL}=10^5 M^{-1}. For simplicity, we consider only 1:1 stoichiometries between target or interferent ions and ionophores (n_I=n_J=1 in Eq. 13). Figure 8.a shows that the LDL is now proportional to the log of β_{JL}. This means that, for β_{JL}=β_{IL} (not shown), ionophores bind the target and interferent ions indiscriminately, giving a membrane response to the primary ion only when $[I_B^+] > [J_B^+]$. In the latter conditions, ionic sites are compensated by equal amounts of IL^+ and JL^+ complexes, whereas the concentration of free ionic species remain negligible. Indeed, in these conditions, cations in the sample are simply indistinguishable. By increasing the strength of the interferent-ionophore complexes (β_{JL}=10^6 M^{-1}), line with right-pointing triangles) the membrane response becomes totally dominated by the effect of the interferent species, except in the inverted Nernstian regime, where the extraction of co-ions X^- from the electrolyte to the ISM dominates the membrane response.

D. Optimum choice of the ionophore concentration

To complement this analysis, we investigate the impact of the total concentration of ionophores $[L_{tot}]$ in the ISM. This parameter is often expressed relative to $[R]$, since the ratio between the two is what defines the capability of the ISM to *buffer* (i.e., to maintain constant) the concentration of the target ions inside this phase [12]. Figure 9 reports a few calibration curves of an ionophore-based ISM, for different ratios $[L_{tot}]/[R]$. In the left panel, the presence of ionophores with concentration that is equal or lower than that of ionic sites yields an improvement on the detection range to target ions with respect to the case without ionophores (line with squares/diamonds vs circles) that is sub-optimal. In fact, despite the detection range is increased, the response is sub-Nernstian and the UDL is lowered. On the other hand, $[L_{tot}]/[R] > 1$ improves the response range which becomes Nernstian for a wider concentration interval of the target ion. Ratios above 2:1 do not lead to appreciable improvement, since the concentration of ionophores is already high enough to successfully buffer the target ions in the ISM.

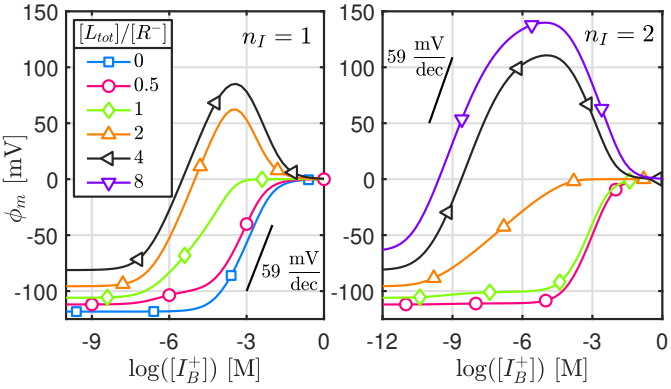

Fig. 9. Calibration curves of cation-selective ISMs at equilibrium with different ratios of $[L_{tot}]/[R] > 1$. The parameter values in the left panel are , $\beta_{JL} = 10^2$ M^{-1}, $n_I = n_J = 1$, $[R^-] = 10$ mM, $[J_B^+] = 0.1$ mM and all the affinity constants are set to 1, whereas in the right panel $\beta_{IL} = 10^{10}$ M^{-2} and $n_I = 2$.

Simulations such as in Fig. 9 quantify the smallest ionophore concentration that gives the best sensor performances. One should note, however, that optimal ratios strongly depend on the stoichiometric coefficients of the ion-ionophore reactions as well as the valence charge of the involved ions [11]. Theoretical approaches have been proposed to use such ratio for optimization of ISM selectivity [32]. In the other way around, experimental data with different $[L_{tot}]/[R]$ can be used, together with simulations, to infer the actual stoichiometric coefficients and binding constants of the chemical reactions [12]. One example is shown in the right panel of Fig. 9, where we repeat the simulations of the left panel but using $n_I = 2$, to show that the optimal ratio changes from 2 to ca. 4. In fact, the stoichiometric coefficient defines how quickly ionophores are consumed by the chemical bound with ions I^+ for increasing concentration of such ions in the sample solution.

E. Effect of the ISM parameters on the detection range and selectivity

So far we have shown which are the main parameters affecting the sensor detection range in ISMs while illustrating the extensive predictive capabilities of the presented models. As shown in Fig. 1.c, the ultimate goal during the design of ISM-based biosensors is that the linear-to-log portion of the sensor characteristics completely covers the concentration range required by the sensor application. Therefore, Fig. 10 suggests a set of intuitive plots, generated with our model, that highlight the visualization of the UDL, LDL and detection range figures of merit. From left to right, each panel shows the detection range (greenish filled area between the UDL

TABLE III
CALCULATED POTENTIOMETRIC SELECTIVITY COEFFICIENTS GIVEN THE PARAMETER VALUES.

$[R]$ (mM)	10	10	10	10	10	10	10	10	10	10	10	10	1
k_I	1	1	1	1	1	1	1	1	0.1	1	1	1	1
k_J	1	1	1	1	1	1	1	1	1	0.1	1	1	1
z_I	1	1	1	1	1	1	1	1	1	1	2	1	1
z_J	1	1	1	1	1	1	1	1	1	1	1	2	1
n_I	1	1	1	1	1	1	2	2	1	1	1	1	1
n_J	1	1	1	1	1	1	1	1	1	1	1	1	1
$\log \beta_{IL}$	4	6	5	5	5	5	10	10	5	5	5	5	5
$\log \beta_{JL}$	0	0	0	4	2	2	2	2	2	2	2	2	2
$[L_{tot}]$ (mM)	20	20	20	20	20	40	40	80	20	20	20	20	20
$\log K_{IJ}^{POT}$ [a]	-2 [c]	-4 [c]	-3 [c]	-1 [c]	-3 [d]	-3 [d]	-6.1 [d]	-6.7 [d]	-2	-4	-1.5	-3.8	-3
$\log K_{IJ}^{POT}$ [b]	-2.1 [c]	-4.1 [c]	-3.1 [c]	-1.4 [c]	-2.7 [d]	-2.9 [d]	-6.1 [d]	-6.8 [d]	-1.7	-3.7	-0.8	-3.7	-3.1

[a] Predictions using Eq. 14. [b] Calculated using [31, Eq. 5] with LDL values extracted from the numerical simulations including ionophores. [c] Parameters values taken from Fig. 8 and, [d], from Fig. 10.

and LDL curves) of an ISM containing ionophores, when changing the concentration of interferent species in the sample electrolyte and the binding association constants β_{IL} and β_{JL} in the ISM, respectively. Other numerical values used in the simulations are: $k_I = k_J = k_X = 1$, $n_I = n_J = 1$, $[R^-] = 10$ mM and $[J_B^+] = 0.1$ mM. From Fig. 10 we observe that the UDL only worsens (decreases) when β_{IL} is increased and remains almost flat otherwise. This in line with the theoretical predictions reported in [33, Eq. 47]. Conversely, the LDL is significantly improved (reduced) with increasing β_{IL} whereas it is worsened with increasing concentration of interferent ions as well as the stability constant β_{JL}. Finally, the detection range follows LDL when the UDL is flat and slightly increases for higher β_{IL}, since the LDL decreases faster than the UDL.

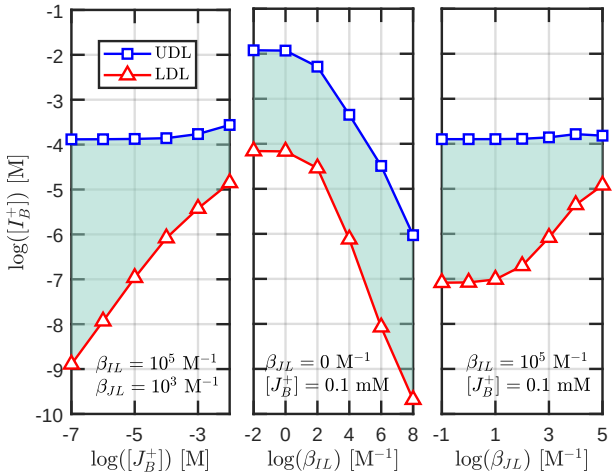

Fig. 10. UDL and LDL trends are plotted against $[J_B^+]$, β_{IL} and β_{JL} in the panels from left to right, respectively. Other parameter values are reported in the text. The shaded area is the detection range.

It is worth noting that the UDL and LDL in Fig. 10 have been calculated following IUPAC convention (see Fig. 1.c). In the particular case of calibration curves with inverted-Nernstian responses (see Fig. 8.a) the UDL was defined by placing the horizontal limit line in correspondence of the inversion peak. This choice leads to slightly shifted results with respect to the convention adopted in [43], where the UDL is defined as the crossing point between the Nernstian and inverted-Nernstian lines.

As previously mentioned in Section II-C, the potentiometric selectivity coefficient can also be used as a FoM for ISM-based sensors. A simple expression for the case of neutral ionophores and monovalent ionic sites reads [32], [33]:

$$\log K_{IJ}^{POT} = \log K_{IJ,0}^{POT} + \frac{z_I}{z_J}\log\beta_{JL} - \log\beta_{IL} + \\ - n_J\frac{z_I}{z_J}\log\left[\left(r - \frac{n_J}{z_J}\right)[R]\right] + n_I\log\left[\left(r - \frac{n_I}{z_I}\right)[R]\right], \quad (14)$$

where we denoted as $\log K_{IJ,0}^{POT}$ the selectivity coefficient without considering ionophores (see Eq. 8) and defined $r = [L_{tot}]/[R]$. The comparison between the numerical simulations performed with our model and the values predicted by Eq. 14 are reported in Table III, for different choices of the ISM parameters, including the examples proposed in Figs. 8-10. The comparison reveals that the theoretical predictions are quite close to the numerical results and that the former are able to capture all the dependencies of the potentiometric selectivity coefficient included in the simulator. However, the discrepancies are not uniformly distributed across the parameters' space, and relatively large errors are obtained in some instances, e.g., for $z_I = 2$ or $\log\beta_{IL} \approx \log\beta_{JL}$.

IV. DISCUSSION AND CONCLUSIONS

In this paper we showed that ISM equilibrium models can be developed using the Poisson-Boltzmann system of equations amenable to extensions including distributed chemical reactions with ionophores. The advantage of our approach with respect to phase boundary models is that the solutions are spatially resolved and extendible to more than one dimension, and allow users to visualize spatial concentration and potential profiles.

Thanks to the inclusion of the spatial dimension and the implementation based on Poisson equation with Neumann/Dirichlet boundary conditions, our models are easy to integrate in simulation tools of the whole sensor device [44], [45], as nowadays relevant for the design of integrated sensor

solutions. The main implementation difficulty remains dealing with non-linearities induced by the PB system of equations, that, coupled with distributed chemical reactions increase the overall complexity, with possible limitations on the number of reactions that can be simultaneously considered. The models are in very good agreement with experimental data in the literature and are useful to characterize the sensor response dependency on the ionic concentrations and the parameters of the ISM. Despite the choice of an equilibrium framework (time is not included) we believe that the proposed approach still conveys useful information to optimize potentiometric sensors.

Based on the simulation results presented in this paper, for idealized ISMs, we summarize below the key points necessary to optimize the LDL, UDL, selectivity and dynamic range of ISM-based electrochemical potentiometric sensors.

When ionophores are not incorporated in the membrane, the ISM design should consider that:

- there is essentially no sensor response without ionic sites;
- the extent of co-ions (e.g., X^- for R^- ionic sites) uptake in the ISM determines the UDL;
- the extent of counter-ions different to the target ions (i.e., J^+) uptake in the ISM determines the LDL;
- The UDL can be improved with i) higher concentrations of ionic sites $[R^-]$, ii) lower affinity constant of the co-ions (e.g., k_X) or iii) lower affinity constant of the target ion (e.g. k_I);
- The LDL can be improved with higher ratio of the target ion affinity constant over the ones of the interferent ionic species, e.g., $k_I > k_J$, or by lowering/increasing the concentration of ionic sites when $z_I < z_J$ or $z_I > z_J$, respectively;
- selectivity among different ions is generally governed by the Hofmeister series.

On the other hand, when ionophores are introduced in the design, one should also consider that:

- ionophores can provide selectivity patterns different from the Hofmeister series;
- if the binding stability of target ion-ionophore complex is high enough (i.e., large β_{IL}), Nernstian sensitivity towards the target species can be achieved even in the presence of high concentrations of interferent ionic species (e.g., $[J_B]$);
- high values of the target ion-ionophore association constant lower the LDL and increase the detection range but worsens the UDL, as they induce co-ion interference;
- The ratio between $[L_{tot}]$ and $[R]$ concentrations in the membrane composition should be optimized according to the ionic valence charges and stoichiometric coefficients of ion-ionophore complexes (usually in 2:1 proportion for monovalent species and 1:1 stoichiometries);
- ion valence charges as well as the number of ionophores that bind a single ion can lead to sub-, super and inverted Nernstian responses also at equilibrium [10], [38].

Acknowledgment

The authors thank the reviewers for their thoughtful comments and efforts towards improving the manuscript.

References

[1] J. Bobacka, A. Ivaska, and A. Lewenstam, "Potentiometric ion sensors," Chem. Rev., vol. 108, no. 2, pp. 329–351, 2008, doi: 10.1021/cr068100w.

[2] E. Zdrachek and E. Bakker, "Potentiometric Sensing," Anal. Chem., vol. 91, no. 1, pp. 2–26, 2019, doi: 10.1021/acs.analchem.8b04681.

[3] P. Bühlmann, S. Yajima, K. Tohda, K. Umezawa, S. Nishizawa, and Y. Umezawa, "Studies on the phase boundaries and the significance of ionic sites of liquid membrane ion-selective electrodes," Electroanalysis, vol. 7, no. 9, pp. 811–816, 1995, doi: 10.1002/elan.1140070905.

[4] A. Bratov, N. Abramova, J. Muñoz, C. Domínguez, S. Alegret, and J. Bartrolí, "Ion sensor with photocurable polyurethane polymer membrane," J. Electrochem. Soc., vol. 141, no. 9, p. L111, 1994, doi: 10.1149/1.2055170.

[5] A. Bratov, N. Abramova, C. Domínguez, and A. Baldi, "Ion-selective field effect transistor (ISFET)-based calcium ion sensor with photocured polyurethane membrane suitable for ionised calcium determination in milk," Anal. Chim. Acta, vol. 408, no. 1, pp. 57–64, 2000, doi: 10.1016/S0003-2670(99)00871-5.

[6] X. Jin, A. Saha, H. Jiang, M. R Oduncu, Q. Yang, S. Sedaghat, D. K. Maize, J. P. Allebach, A. Shakouri, N. J. Glassmaker, A. Wei, R. Rahimi, and M. Alam, "Steady-State and Transient Performance of Ion-Sensitive Electrodes Suitable for Wearable and Implantable Electrochemical Sensing," IEEE Trans. Biomed. Eng., pp. 1–1, 2021, doi: 10.1109/TBME.2021.3087444.

[7] B. P. Nicolsky, "Theory of the glass electrode. I. Theoretical," J. Phys. Chem. (U.S.S.R.), vol. 10, pp. 495–503, 1937.

[8] G. Eisenman, Ion-selective electrodes: proceedings. US National Bureau of Standards, 1969, vol. 13.

[9] S. Amemiya, P. Bühlmann, and Y. Umezawa, "A phase boundary potential model for apparently "twice-nernstian" responses of liquid membrane ion-selective electrodes," Anal. Chem., vol. 70, no. 3, pp. 445–454, 1998, doi: 10.1021/ac9710184.

[10] S. Amemiya, P. Bühlmann, and K. Odashima, "A Generalized Model for Apparently "Non-Nernstian" Equilibrium Responses of Ionophore-Based Ion-Selective Electrodes. 1. Independent Complexation of the Ionophore with Primary and Secondary Ions," Anal. Chem., vol. 75, no. 14, pp. 3329–3339, 2003, doi: 10.1021/ac026471g.

[11] E. Bakker, P. Bühlmann, and E. Pretsch, "The phase-boundary potential model," Talanta, vol. 63, no. 1, pp. 3–20, 2004, doi: 10.1016/j.talanta.2003.10.006.

[12] P. Bühlmann and L. D. Chen, "Ion-selective electrodes with ionophore-doped sensing membranes," Supramol. Chem., 2012, doi: 10.1002/9780470661345.smc097.

[13] K. N. Mikhelson, Ion-selective electrodes. Springer, 2013, vol. 81, doi: 10.1007/978-3-642-36886-8.

[14] R. Buck and E. Lindner, "IUPAC 46/89 Document "Recommendations for Nomenclature of Ion-Selective Electrodes"," Pure Appl. Chem, vol. 66, pp. 2527–2536, 1994, doi: 10.1351/pac199466122527.

[15] A. Hulanicki and A. Lewenstam, "Interpretation of selectivity coefficients of solid-state ion-selective electrodes by means of the diffusion-layer model," Talanta, vol. 24, no. 3, pp. 171–175, 1977. [Online]. Available: https://www.sciencedirect.com/science/article/pii/0039914077800842

[16] A. Lewenstam, A. Hulanicki, and T. Sokalski, "Response mechanism of solid-state ion-selective electrodes in the presence of interfering ions," Analytical Chemistry, vol. 59, no. 11, pp. 1539–1544, 1987.

[17] T. Sokalski and A. Lewenstam, "Application of Nernst–Planck and Poisson equations for interpretation of liquid-junction and membrane potentials in real-time and space domains," Electrochem. commun., vol. 3, no. 3, pp. 107–112, 2001, doi: 10.1016/S1388-2481(01)00110-2.

[18] P. Lingenfelter, T. Sokalski, and A. Lewenstam, "Numerical solution of the coupled Nernst-Planck and Poisson equations for ion-selective membrane potentials," Materials Research Society Symposium - Proceedings, vol. 752, pp. 193–198, 2003.

[19] P. Lingenfelter, I. Bedlechowicz-Sliwakowska, T. Sokalski, M. Maj-Zurawska, and A. Lewenstam, "Time-dependent phenomena in the potential response of ion-selective electrodes treated by the Nernst-Planck-Poisson model. 1. Intramembrane processes and selectivity," Analytical Chemistry, vol. 78, no. 19, pp. 6783–6791, 2006.

[20] T. Sokalski, W. Kucza, M. Danielewski, and A. Lewenstam, "Time-Dependent Phenomena in the Potential Response of Ion-Selective Electrodes Treated by the Nernst-Planck-Poisson Model. Part 2: Transmembrane Processes and Detection Limit," Anal. Chem., vol. 81, no. 12, pp. 5016–5022, 2009, doi: 10.1021/ac900490c.

[21] J. J. Jasielec, G. Lisak, M. Wagner, T. Sokalski, and A. Lewenstam, "Nernst-Planck-Poisson Model for the Description of Behaviour of Solid-Contact Ion-Selective Electrodes at Low Analyte Concentration," Electroanalysis, vol. 25, no. 1, pp. 133–140, 2013.

[22] L. J. Mele, P. Palestri, and L. Selmi, "Device simulations of ion-sensitive fets with arbitrary surface chemical reactions," in 2021 Joint International EUROSOI Workshop and International Conference on Ultimate Integration on Silicon (EuroSOI-ULIS), 2021, pp. 1–4, doi: 10.1109/EuroSOI-ULIS53016.2021.9560696.

[23] M. Giugliano, "mgiugliano/infet_project: First release," Feb. 2021, doi: 10.5281/zenodo.4497817. [Online]. Available: https://github.com/mgiugliano/infet_project/tree/first

[24] F. Hofmeister, "Concerning regularities in the protein-precipitating effects of salts and the relationship of these effects to the physiological behaviour of salts," Arch. Exp. Pathol. Pharmacol, vol. 24, pp. 247–260, 1888.

[25] F. Pittino and L. Selmi, "Use and comparative assessment of the CVFEM method for Poisson-Boltzmann and Poisson-Nernst-Planck three dimensional simulations of impedimetric nano-biosensors operated in the DC and AC small signal regimes," Comput Methods Appl Mech Eng, vol. 278, pp. 902–923, 2014, doi: 10.1016/j.cma.2014.06.006.

[26] "APBS & PDB2PQR," https://www.poissonboltzmann.org/, accessed: 2021-10-18.

[27] "Nernst-Planck-Poisson (NPP) Model, JEDS 2.0," https://home.agh.edu.pl/~jasielec/software/npp, accessed: 2022-02-15.

[28] R. Armstrong and G. Horvai, "Properties of PVC based membranes used in ion-selective electrodes," Electrochim. Acta, vol. 35, no. 1, pp. 1–7, 1990, doi: 10.1016/0013-4686(90)85028-L.

[29] A. Ceresa and E. Pretsch, "Determination of formal complex formation constants of various Pb^{2+} ionophores in the sensor membrane phase," Anal. Chim. Acta, vol. 395, no. 1, pp. 41–52, 1999, doi: 10.1016/S0003-2670(99)00311-6.

[30] E. Lindner and Y. Umezawa, "Performance evaluation criteria for preparation and measurement of macro- and microfabricated ion-selective electrodes (IUPAC Technical Report)," Pure and Applied Chemistry, vol. 80, no. 1, pp. 85–104, 2008.

[31] E. Bakker, E. Pretsch, and P. Bühlmann, "Selectivity of potentiometric ion sensors," Analytical Chemistry, vol. 72, no. 6, pp. 1127–1133, 2000.

[32] S. Amemiya, P. Bühlmann, E. Pretsch, B. Rusterholz, and Y. Umezawa, "Cationic or anionic sites? Selectivity optimization of ion-selective electrodes based on charged ionophores," Analytical Chemistry, vol. 72, no. 7, pp. 1618–1631, 2000.

[33] E. Bakker, P. Bühlmann, and E. Pretsch, "Carrier-Based Ion-Selective Electrodes and Bulk Optodes. 1. General Characteristics," Chemical Reviews, vol. 97, no. 8, pp. 3083–3132, 1997.

[34] R. Eugster, P. M. Gehrig, W. E. Morf, U. E. Spichiger, and W. Simon, "Selectivity-Modifying influence of Anionic Sites in Neutral-Carrier-Based Membrane Electrodes," Analytical Chemistry, vol. 63, no. 20, pp. 2285–2289, 1991.

[35] S. Wilke and T. Zerihun, "Standard Gibbs energies of ion transfer across the water — 2-nitrophenyl octyl ether interface," Journal of Electroanalytical Chemistry, vol. 515, no. 1-2, pp. 52–60, 2001, doi: 10.1016/S0022-0728(01)00640-4.

[36] I. Yilmaz, L. D. Chen, X. V. Chen, E. L. Anderson, R. C. Da Costa, J. A. Gladysz, and P. Bühlmann, "Potentiometric Selectivities of Ionophore-Doped Ion-Selective Membranes: Concurrent Presence of Primary Ion or Interfering Ion Complexes of Multiple Stoichiometries," Anal. Chem., vol. 91, no. 3, pp. 2409–2417, 2019, doi: 10.1021/acs.analchem.8b05196.

[37] P. Bühlmann and Y. Umezawa, "Apparently "Non-Nernstian" Equilibrium Responses Based on Complexation Between the Primary Ion and a Secondary Ion in the Liquid ISE Membrane," Electroanalysis, vol. 11, no. 10-11, pp. 687–693, 1999, doi: 10.1002/(SICI)1521-4109(199907)11:10/11⟨687::AID-ELAN687⟩3.0.CO;2-C.

[38] L. J. Mele, P. Palestri, and L. Selmi, "Modeling Selectivity and Cross-sensitivity in membrane-based potentiometric sensors," in 2020 Joint International EUROSOI Workshop and International Conference on Ultimate Integration on Silicon (EUROSOI-ULIS), 2020, pp. 1–4, doi: 10.1109/EUROSOI-ULIS49407.2020.9365285.

[39] Y. Qin, Y. Mi, and E. Bakker, "Determination of complex formation constants of 18 neutral alkali and alkaline earth metal ionophores in poly (vinyl chloride) sensing membranes plasticized with bis (2-ethylhexyl) sebacate and o-nitrophenyloctylether," Analytica chimica acta, vol. 421, no. 2, pp. 207–220, 2000, doi: 10.1016/S0003-2670(00)01038-2.

[40] P. Bühlmann, E. Pretsch, and E. Bakker, "Carrier-based ion-selective electrodes and bulk optodes. 2. Ionophores for potentiometric and optical sensors," Chem. Rev., vol. 98, no. 4, pp. 1593–1688, 1998, doi: 10.1021/cr970113+.

[41] H. Freiser, Ion-selective electrodes in Anal. Chem. Springer Science & Business Media, 2012.

[42] A. D. Ivanova, E. S. Koltashova, E. V. Solovyeva, M. A. Peshkova, and K. N. Mikhelson, "Impact of the electrolyte co-extraction to the response of the ionophore-based ion-selective electrodes," Electrochim. Acta, vol. 213, pp. 439–446, 2016, doi: 10.1016/j.electacta.2016.07.142.

[43] E. Bakker, A. Xu, and E. Pretsch, "Optimum composition of neutral carrier based pH electrodes," Analytica chimica acta, vol. 295, no. 3, pp. 253–262, 1994.

[44] COMSOL Multiphysics user manual, COMSOL Inc., Sweden, 2021.

[45] Synopsys Sentaurus Device simulator user manual, Synopsis Inc., Mountain View, CA, USA, 2016.

Leandro Julian Mele (GSM'17–M'20) received the Ph.D. degree in electronic engineering from the University of Udine, Udine, Italy, in 2021. He currently holds a post-doctoral position with the University of Udine, Italy. His research interests include electrochemical modeling of performance and noise for electronic biosensors, emerging ion-to-electronic interfaces using conductive polymers and bio-actuators. In 2015, he received the Best Graduate award for the B.S. in Electronic Engineering.

Pierpaolo Palestri (M'05–SM'13) received the Laurea degree in electronic engineering from the University of Bologna, Bologna, Italy, in 1998, and the Ph.D. degree in electronic engineering from the University of Udine, Udine, Italy, in 2003. In 2000 and 2001, he held a post-doctoral position with Bell Laboratories, Murray Hill, NJ, USA. He is currently an Associate Professor with the University of Udine. His research interests include the modeling of nanoscale devices and sensors, as well as the design of integrated circuits for high-frequency applications. He has co-authored about 250 paper in international journal and conferences with peer review.

Muhammad A. Alam (M'96–SM'01–F'06) received the Ph.D. degree from Purdue University, West Lafayette, IN, USA, in 1995. He was with Bell Laboratories, Murray Hill, NJ, USA, where he was involved in laser dynamics, crystal growth, and CMOS reliability. Since 2004, he has been with Purdue University, where he currently holds the Jai N Gupta Professorship of Electrical Engineering. His research interests include physics, simulation, characterization and technology of classical and emerging electronic devices, including reliability of scaled MOSFET, theoretical foundation of nano-bio sensors, and atom-to-farm performance and modeling of solar cells. His work has been recognized by 2006 IEEE Kiyo Tomiyasu Medal, 2015 SRC Technical Excellence Award, and 2018 IEEE EDS Education Award.

Luca Selmi (M'01–SM'09–F'15) received the Ph.D. degree in electronic engineering from the University of Bologna, Italy, in 1992. Since 2000, he has been a Professor of electronics with University of Udine, and since 2017 with University of Modena and Reggio Emilia. His research interests covered simulation, modeling, and characterization of nanoscale CMOS transistors and NVM, with emphasis on hot-carrier effects, quasiballistic transport, Monte Carlo simulation, and recently nanoelectronic ISFET and impedance spectroscopy (bio)sensors. He was a TPC member of IEEE IEDM and VLSI Symposium, and associate Editor of IEEE EDL.